Praseodymium sorption on Laminaria digitata algal beads and foams

Shengye Wang, Mohammed F. Hamza, Thierry Vincent, Catherine Faur, Eric Guibal

Praseodymium sorption on *Laminaria digitata* algal beads and foams

Shengye Wang [a], Mohammed F. Hamza [b], Thierry Vincent [a], Catherine Faur [c], Eric Guibal [a,*]

[a] *Ecole des mines d'Alès, Centre des Matériaux des Mines d'Alès, Pôle Matériaux Polymères Avancés, 6 avenue de Clavières, F-30319 Alès cedex, France* [b] *Nuclear Materials Authority, 530 El-Maadi, Cairo, Egypt*

[c] *Institut Européen des Membranes-IEM (UMR 5635, Université de Montpellier, ENSM, CNRS), Place Eugène Bataillon, 34095 Montpellier Cedex 5, France*

A B S T R A C T

Algal (*Laminaria digitata*) beads and algal foams have been prepared by a new synthesis mode and the sorbents were tested for praseodymium sorption in batch and fixed-bed like systems (recirculation or one-pass modes), respectively. Metal binding occurs through ion-exchange with Ca(II) ions used for iono-tropic gelation of alginate contained in the algal biomass and eventually with protons. Sorption isotherms at pH 4 are described by the Langmuir and the Sips equations with maximum sorption capacities close to 110–120 mg Pr g^{-1}. Uptake kinetics are fitted by the pseudo-second order reaction rate equation for both beads and foams; in the case of beads the Crank equation also gives good fit of experimental data. Metal is successfully desorbed using 2 M HCl/0.05 M $CaCl_2$ solutions and the sorbent can be efficiently re-used for a minimum of 5 cycles with negligible decrease in sorption/desorption properties and appreciable con-centrating effect (around 8–10 times the initial metal concentration). Tested in continuous mode, the algal foam shows typical breakthrough curves that are fitted by the Yan method; desorption is also effi-cient and allows under the best conditions to achieve a concentration factor close to 8.

Keywords:
Brown algae
Praseodymium
Ion-exchange
Sorption isotherm
Uptake kinetics
Beads
Foams
Breakthrough columns
Metal desorption
FTIR
SEM-EDX

G R A P H I C A L A B S T R A C T

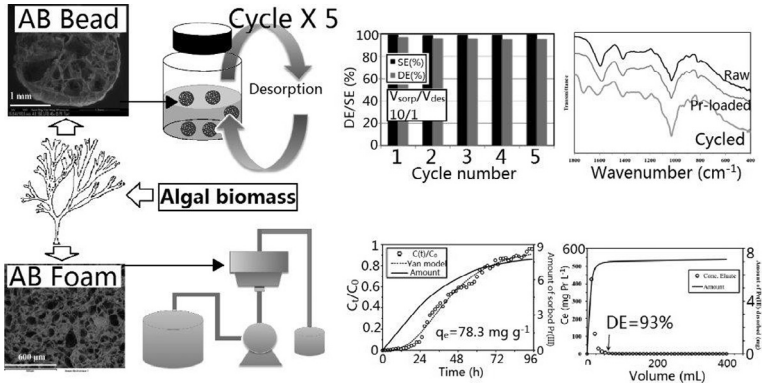

1. Introduction

Rare earth elements (REEs) are widely used in High-Tech appli-cations (photo-electronics, electronics, super-magnets, special

* Corresponding author.
E-mail address: Eric.Guibal@mines-ales.fr (E. Guibal).

alloys, etc.) [1,2]. The rarefaction of the resource and the geopolitical issues associated to the distribution of production areas may explain the incentive policies for recovering these strategic and critical metals from sub-marginal sources [1,3] and their recycling from spent materials [4–6], and more specifically from waste electric and electronic equipment (WEEE) [7,8]. The leaching of ores or waste materials generates acidic solutions containing base metals and precious/critical metals such as rare earth elements [9,10]; these metals can be valorized by selective precipitation [3], solvent extraction [3,11], membrane solvent extraction [12], or sorption [13] using resins [14], chemically modified inorganic sorbents [15], and biosorbents [16,17].

Alginate is a polysaccharide extracted from algal biomass (mainly brown algae) [18]. The carboxylic acid groups (i.e., guluronic acid and mannuronic acid) are the main reactive groups that are involved in metal binding [19–27]. Raw alginate and chemically modified biopolymer have been investigated for the sorption of rare earth elements [28–33]. However, the extraction of alginate has environmental impact and increases the relative cost of the sorbent. Several studies have shown the efficiency of brown algal biomass for heavy metal removal [34–36] and REEs recovery [16,37–41]. The main drawback in using these materials is due to the ribbon-like structure of the algal biomass and its swelling that may strongly impact their application in continuous systems (such as fixed-bed columns) with pressure head loss, and blocking effects. For these reasons several studies have been dedicated to the immobilization of algal biomass in a suitable polymer or biopolymer to form hydrogel beads with enhanced hydrodynamic behavior [42–46]. However, these processes usually require the incorporation of alginate or other polymer for the encapsulation of the selected biosorbents with additional cost. Recently, a new method has been used for the synthesis of algal beads and relevant composites with a one-pot extraction and shaping of alginate fraction of the algal biomass: the process was used for preparing algal-biomass beads and composite sorbents (associating algal biomass and glutaraldehyde cross-linked polyethyleneimine) [47–49].

The method consists of the mild-alkaline extraction of alginate-based compound from the algal biomass and the further distribution of the preparation suspension into an ionotropic gelation solution. This technique was used for elaborating algal biomass beads (AB beads) without addition of encapsulating agent. The synthesis of highly macro-porous sponges/foams has been documented for tissue engineering, growth of biological cells [50] but also for the elaboration of original materials like reactive sponges [51] that can be used for absorbing contaminated water: the reaction takes place in the sponge before a wriggling step allows removing decontaminated water and concentrating in the support the toxic metal. These materials are characterized as highly macro-porous supports with high percolating properties that can be used as reactive filters [52,53]. The concept has been used for designing in this work algal biomass foams (AB foams) that will be used for the recovery of a REE and the sorption properties are compared with the sorption behavior of AB beads.

The study is focused on the sorption of praseodymium and includes the study of pH effect, the investigation of uptake kinetics using AB beads (air-dried, AD, and freeze-dried, FD), the sorption isotherms are then compared for AB beads and AB foams. The desorption kinetics are investigated before investigating the recycling of the sorbent (successive sorption/desorption cycles) and also the effect of the volume ratio between sorption volume and desorption volume on the concentrating effect and desorption efficiency (optimization of desorption process). Finally the continuous sorption and desorption of Pr(III) were investigated in a fixed-bed mode using AB foams. The materials have been characterized using FTIR spectroscopy, scanning electron microscopy (morphology) and SEM-EDX (energy dispersive X-ray) analysis (map distribution of elements) for identifying reactive groups and evaluating the physico-chemical degradation of the material during the alternating sorption/desorption cycles.

2. Materials and methods

2.1. Materials

Laminaria digitata brown alga was supplied by Setalg (Pleubian, France). Algal biomass was washed, dried at 50 °C overnight and grinded (size fraction below 250 μm was used). The procedure described by McHugh [54] and modified by Bertagnolli et al. [55] was used for the extraction and quantification of alginate from algal biomass. NMR analysis [56] was used for the characterization of mannuronic acid (M)/guluronic acid (G) contents in extracted alginate (i.e., M/G: 0.62/0.38) [47].

Calcium chloride (99.5+, %), HCOOH (99+, %) were supplied by Chem Lab (Chem Lab NV, Zedelgem, Belgium), Sigma-Aldrich (Saint-Louis (MO), USA. Calcium carbonate (99+,%) was purchased from Sigma-Aldrich (Taufkirchen, Germany). Praseodymium chloride was supplied by Alfa Aesar (Thermo Fisher (Kandel) GmbH, Karlsruhe, Germany).

2.2. Synthesis of beads and foams

Algal biomass (40 g, dry weight) and Na_2CO_3 (8 g, d.w.) were introduced into 1152 mL of demineralized water. The suspension was maintained at 50 °C for 24 h. In the next step, $CaCO_3$ powder (8 g) was homogeneously dispersed in the suspension under strong stirring. The suspension was then wisely dropped into a $CaCl_2$/HCOOH solution (1%, w/w for both salt and acid). The beads formed by ionotropic gelation were kept under agitation (150 rpm) for 24 h: the slow reaction between formic acid and calcium carbonate releases Ca(II) ions that cross-link the alginate extracted from algal biomass (reaction between carboxylic groups of the biopolymer and calcium ions); in addition, CO_2 bubbles are produced that contribute to produce internal porosity. The last step consisted of controlling the pH of the solution to 4. After 24 h of contact the beads were carefully washed with demineralized water before being freeze-dried (−52 °C, 0.1 mbar) for 2 days. Freeze-drying allows maintaining, at least partially, the porous structure of the beads (FD) contrary to beads that were air-dried (AD).

Ionotropic gelation was also applied for the synthesis of algal foams. Fifteen g of *Laminaria digitata* (dry weight) and 3 g of Na_2CO_3 were mixed into 576 mL of pure water before being heated at 50 °C for 24 h in an oven. Six hundred milliliters of algal suspension were mixed with 20 mL of a homogeneous suspension of $CaCO_3$ suspension (1%, w/w). The homogeneous suspension was rapidly dropped into disc molds (50 mm, diameter). The molds were frozen at −80 °C for 1 h before being freeze-dried (−52 °C, 0.1 mbar) for 2 days. Thereafter dried foams were soaked into a solution containing both $CaCl_2$ (1%, w/w) and HCOOH (1%, w/w) under slow shaking (20 rpm) for 24 h. The foams were then carefully washed with demineralized water (4 steps, with 4 L of water) and freeze-dried (−52 °C, 0.1 mbar) for 24 h.

2.3. Characterization of materials

The size of the beads (dried, freeze-dried, and soaked) were determined by optical photographs and statistical analysis on a 20-samples lot. Scanning electron microscopy (SEM) and SEM-EDX (SEM coupled with energy dispersive X-ray diffraction analysis) were performed using an environmental scanning electron microscope Quanta FEG 200 (FEI France, Thermo Fisher Scientific, Mérignac, France), equipped with an Oxford Inca 350 energy

dispersive X-ray micro-analyzer (Oxford Instruments France, Saclay, France). FT-IR spectrometry analysis was performed in the range 4000–400 cm^{-1} using an FTIR-ATR (Attenuated Total Reflectance tool) Bruker VERTEX70 spectrometer (Bruker, Germany).

For the physico-chemical characterization of Pr(III) sorption on algal beads, the beads were mixed for 48 h with 200 mg Pr L^{-1} solution (at pH 4, controlled by either 1 M NaOH or nitric acid solutions) with a sorbent dosage (SD) of 200 mg L^{-1}. For the characterization of recycled material (5 sorption/desorption steps), the following experimental conditions have been used; sorption: C_0: 25 mg Pr L^{-1}; SD: 0.4 g L^{-1}; contact time: 24 h – desorption: 2 M HCl/0.05 M $CaCl_2$; SD: 0.4 g L^{-1}; contact time: 2 h. Similar procedure was used for loading AB foams and the Pr(III) loading on the sorbents was close to the maximum sorption capacity (i.e., about 100 mg Pr g^{-1}).

The pH_{ZPC} of the sorbent was determined by titration [57]. One hundred and fifty mg of sorbent were mixed with a 0.1 M NaCl solution for 48 h; the initial pHs (pH_0) were varied between 2 and 8, the final pH (pH_{eq}) was recorded and plotted against initial pH; the pH_{ZPC} corresponds to the pH were the plot crosses the first bisectrice (i.e., $pH_{eq} = pH_0$).

The apparent density and porosity of the foams were characterized by pycnometer measurements using ethanol as the soaking agent. Two different processes were tested using either foam discs (as produced) and geometrically cut materials (measuring the dimensions with a vernier caliper).

2.4. Sorption tests

For the sorption experiments performed on algal biomass beads (AB beads) the sorbent was mixed with Pr(III) solutions at fixed values of pH (controlled with 1 M NaOH or HNO_3 solutions) for 48 h. The pH was not adjusted during the experiment but was systematically monitored at equilibrium (using a pH-meter cyber scan pH 6000 (Eutech instruments, Nijkerk, Netherlands). Experiments were performed at 20 °C ± 1 °C. Experimental conditions such as pH, sorbent dosage (SD = m/V, mg L^{-1}, m: g; V: L), metal concentration (C_0: mg Pr L^{-1}), contact time were varied for carrying out pH effect, sorption isotherms, uptake kinetics: full experimental conditions are systematically reported in the caption of the figures (see below). Samples were collected, filtrated on 1.2 μm pore size membranes and analyzed for residual metal concentration (C(t) or C_{eq}, mg Pr L^{-1}, or mmol Pr L^{-1}) using an ICP-AES spectrometer (inductively coupled plasma atomic emission spectrometer, Horiba France, Jobin-Yvon Activa M, Longjumeau, France). The mass balance equation was used for calculating the amount of metal immobilized on the sorbent (q, mg Pr g^{-1} or mmol Pr g^{-1}): $q=(C_0 - C_{eq})V/m$. For desorption studies similar methods were used; the eluent was, in most cases, 2 M HCl/0.05 M $CaCl_2$ solution. The addition of calcium chloride in the eluent is supposed to reinforce the stability of the sorbent. The mass balance between sorption and desorption steps allowed calculating desorption efficiency. In order to evaluate the concentration effect during the desorption, two different conditions of volume ratio ($V_{sorption}/V_{desorption}$) were considered: $V_{sorpt.}/V_{des.} = 1$ (desorption efficiency) and $V_{sorpt.}/V_{des.} = 10$ (concentration effect).

Experiments with AB foams were carried out by disposing the foam (which was cut with a die to a diameter of 25 mm) into a filter membrane holder (Swinnex, Ø 25 mm, Millipore, Merck Chimie SAS, Fontenay sous Bois, France). Metal ions solutions were pumped (using a MasterFlex peristaltic pump) through the immobilized AB foams on a recirculation mode at high flow rate (i.e., 5 mL min^{-1}; to prevent the formation of internal air bubbles, and preferential channels). Specific experiments were performed in direct flow mode (without solution recirculation) at low flow rate (i.e., 0.2 mL min^{-1}) to simulate fixed-bed system: a sample collector was connected to the outlet of the immobilized AB foam. The filtration bed consisted of a single foam disc (m: 98.7 mg (d.w.), Ø: 25 mm; height: ≈2.45 ± 0.11 mm).

The sorbents were stored as dry beads (or foams) and were soaked in water overnight just before use.

Note: Selected sorption tests were duplicated and the variation was considered negligible when the standard deviation was less than 6%. For example, a repeatability test carried out on breakthrough curves is presented at the end of the Additional Material Section.

2.5. Modeling of sorption processes

Conventional equations used for modeling sorption processes such as uptake kinetics (pseudo-first order rate equation [58], PFORE, pseudo-second order rate equation [59], PSORE, and Crank equation [60]), sorption isotherms [61] (Langmuir and Sips equations), and breakthrough columns (Yan equation [62]) are summarized in the Additional Material Section.

3. Results and discussion

3.1. Characterization of materials

The size characteristics of AB beads have been previously reported [47,63]: the size of dried beads and rehydrated beads strongly depends on the drying mode. The freeze-dried AB beads have very close particle size before and after rehydration: 2.64 ± 0.16 mm and 2.50 ± 0.22 mm, respectively. The air-drying has a much stronger impact on the size of sorbent particles: dried particles have a diameter of 0.99 ± 0.10 mm while after rehydration the size significantly increases to 1.46 ± 0.13 mm (though it remains much lower than the soaked FD beads). The air-drying irreversibly affects the porosity of the algal hydrogel while the freeze-drying controls the capillary forces during the drying step and the collapse of the porous structure is reduced and hardly affects the size of the objects. The size reduction with air-drying may have an important impact on accessibility to internal reactive groups and to kinetic profiles. However, this effect is relatively limited for the binding of metal cations such as Pb(II) and Cu(II) [47], while its impact is more significant for large size metal anions such as hexachloroplatinate and tetrachloropalladate anions [63].

Fig. 1 shows the internal porosity of AB beads and the morphology of AB foams. AB beads have a roughly spherical shape with very large internal porosity (up to 500 μm): the production of CO_2 during the reaction of calcium carbonate with formic acid during the synthesis may explain this porosity together with the proper ionotropic gelation mechanism that segregates the water from polymer scaffold. The AB foams also shows a large internal porosity (up to 150 μm; i.e., smaller than the largest holes in the AB beads) that clearly explain the good percolating properties of the thin discs. It is noteworthy that the freeze-drying may contribute to break some internal foils in the scaffold: the porosity is also clearly interconnected. The pycnometer measurements allowed calculating the density (0.492 ± 0.066 g cm^{-3}), the bulk density (0.0326 ± 0.000375 g cm^{-3}), and the porosity of the foam (93.33 ± 1.03%).

Figs. AM1–AM3 (see Additional Material Section) shows the porous structure, the EDX analysis and the map distribution of main elements for AB beads before, after Pr(III) sorption and after 5 cycles of sorption/desorption. The raw material (Fig. AM1) is characterized by the presence of C and O elements (organic tracers), S element (sulfated polysaccharides such as fucoidans, carrageenans, which are present in brown algae). Small amounts of Si element (probably associated to impurities, diatomaceous

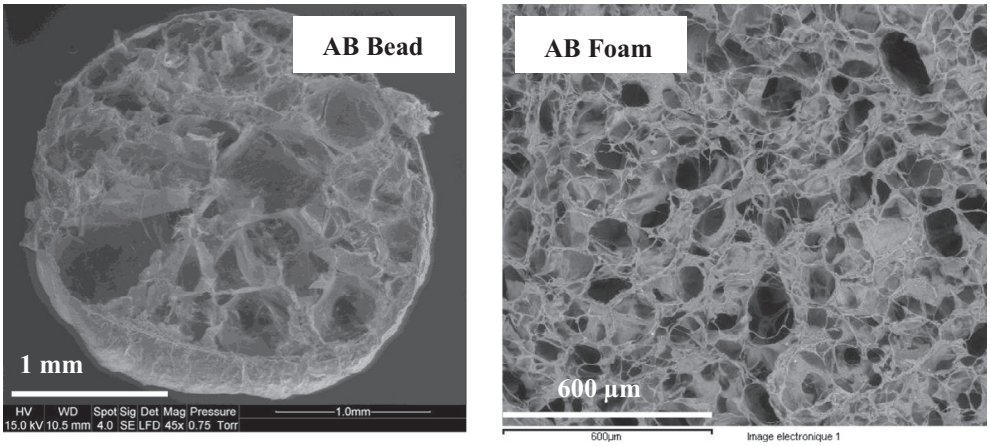

Fig. 1. Porous structure of Algal Biomass sorbents (SEM micrographs).

residues), Na and Cl elements (residues of the extraction/shaping process) are also present. Ca element is typically the tracer of the ionotropic gelation process. These elements are homogeneously distributed in the section of AB bead. After Pr(III) sorption the morphology of the beads does not significantly change (Fig. AM2), contrary to the elemental composition: the Ca peaks on the EDX analysis almost disappears and are replaced with the signals of Pr element. The sorption of Pr(III) clearly involves an ion-exchange mechanism between Pr(III) and Ca(II). Pr(III) distribution is also homogeneous in the sorbent: the material is porous enough to make all internal reactive groups in the sorbent accessible for Pr (III). The SEM-EDX analysis on AB beads after 5 successive sorption/desorption cycles shows that the structure of the material remains stable, that Ca element re-appears in the biosorbents while Pr element almost completely disappears: residual metal concentration in the beads does not exceed 9.2 mg Pr g^{-1}, corresponding to the reversal ion-exchange between Ca(II) and Pr(III) (compared to the sorption step). Ca element is homogeneously distributed in the complete section of the AB bead. Similar trends are observed in the case of AB foams (Figs. AM4–5): the elements are homogeneously distributed and metal binding occurs through ion-exchange between Ca(II) and Pr(III).

The analysis of these three materials (raw, after Pr(III) sorption and after 5 sorption/desorption cycles) was also performed by FTIR spectroscopy (Fig. AM6, wavenumber range: 1800–400 cm^{-1}; see Additional Material Section). The FTIR spectra of the sorbent before and after Pr(III) sorption show very similar profiles. The assignments of the main bands in spectra are reported in Table AM1 (see Additional Material Section). After Pr(III) sorption the main changes are associated to a slight shift of the band at 1595 cm^{-1} (assigned to $\nu_{asymm}(COO^-)$, [64]) toward lower wavenumber (i.e., 1582 cm^{-1}). It is noteworthy that the width of this band and that of the band at 1415 cm^{-1} (assigned to $\nu_{symm}(COO^-)$) are slightly broadened after metal binding. Papageorgiu et al. [64] discuss the mode of interaction of different metal ions with carboxylate groups alginate (bidentate chelating coordination, bidentate bridging coordination or unidentate coordination) in relation with the difference in the wavenumbers for asymmetric and symmetric stretching vibrations of carboxylate groups ($\Delta\nu(COO^-)$). When the $\Delta\nu$(COO/Me) is lower than $\Delta\nu$(COO/Na) the binding mechanism is a bidentate chelating coordination; on the other hand, when the two $\Delta\nu$(COO) are similar the mechanisms involves bidentate bridging coordination, while metal binding mechanism consists of unidentate coordination when the $\Delta\nu$(COO/Me) is lower than $\Delta\nu$(COO/Na). In the binding of Ca(II), Cu(II), Cd(II), Pb(II), Ni(II) and Zn(II) they found values for $\Delta\nu$(COO/Me) that are comparable or slightly slower than the corresponding value for Na(I) (i.e., close to 192 cm^{-1}). In the case of Pr(III) binding on AB beads the $\Delta\nu$(COO/Pr) is close to 167 cm^{-1} (i.e.;, similar to the values found for Pb(II) and Cd(II) by alginate) lower than the value for Na(I) meaning that the unidentate bridging coordination would explain metal binding. However, they deeply discuss the mechanism and explain that several mechanisms may be involved due to the presence of mannuronic acid and guluronic acid that differently react with metal ions involving a pseudo-bridging unidentate mechanism for polyguluronate-metal complexes and a bidentate bridging coordination for metal binding in polymannuronic-metal complexes. The complexity of the interaction mechanisms is even more complex in the case of algal biomass due to the presence of additional groups that may be involved in metal uptake (including amine groups present on some internal cell constituents and fucoidan-based compounds). In the case of the sorbent that was recycled 5 times, many changes show that the material was chemically modified by the successive sorption/desorption treatments. A new peak is appearing at 1726 cm^{-1} (which was assigned to the stretching vibration of C=O bond); this is probably associated to the degradation of carboxylic groups. In addition, the asymmetric stretching of COO^- bond is shifted toward higher wavenumbers (i.e., 1620 cm^{-1}): the stability of the "macroscopic composition" (identified on SEM-EDX analysis) is not confirmed by the FTIR characterization. Other changes consist of the appearance of a shoulder at around 1520 cm^{-1}, and a band at 1234 cm^{-1} (which was assigned to the stretching of C-O bonds). In addition; some weak peaks around 870 cm^{-1}, 930 cm^{-1} and 1050 cm^{-1} are little more marked in the recycled material. Most of praseodymium binding occurs on carboxylic/carboxylate groups through coordination; the succession of sorption/desorption steps affects the chemical structure of the sorbent (especially these groups that are involved in metal binding). Further experiments will show how this chemical modification may affect (or not) the sorption performance (see below).

The so-called pH drift method [57] was used for evaluating the pH_{ZPC} of the sorbent (not shown). The value is close to 5.09 for AB foams and 4.84 for beads. This means that below pH 5, the sorbents are roughly positively charged.

3.2. pH effect

The effect of pH was investigated using beads only; indeed, foam- and bead-shaped materials were characterized by very close pH_{ZPC}. Fig. 2 shows the effect of pH on sorption capacity and sorption efficiency. At pH close to 1.5, sorption capacity is

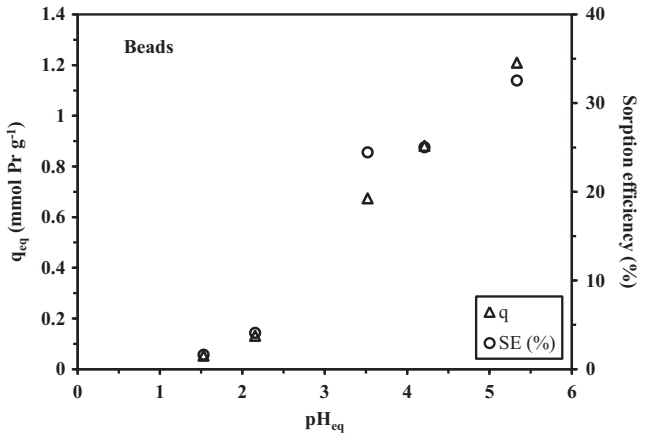

Fig. 2. pH effect on Pr(III) sorption on Algal Biomass beads – sorption efficiencies and sorption capacities *vs.* equilibrium pH (C_0: 100 mg Pr(III) L^{-1}; Sorbent dosage, SD: 0.2 g L^{-1}; contact time: 48 h; T: 20 °C).

negligible (around 5 mg Pr g^{-1}). Increasing pH improves Pr(III) sorption: the sorption capacity linearly increases. This may be explained by the progressive decrease of the competition effect of protons. The pH_{ZPC} being close to 5.1, reactive groups are protonated and metal sorption may occurs through ion-exchange between Pr(III) cations and the protons and Ca(II) cations bound to the sorbent (sulfonic/sulfated groups, amine groups, carboxylate groups). An excess of protons in acidic solution competes against Pr(III) cations for binding and ion-exchange on sorbent surface. The pK_as of mannuronic acid and guluronic acid have been determined by titration close to 3.38 and 3.65, respectively [65]. These values are below the pH_{ZPC}; the presence of other functional groups induces different and more complex acid-base behavior. Fig. AM7 (see Additional Material Section) plots the distribution ratio (calculated by the ratio $D = q_{eq}/C_{eq}$; L g^{-1}) *vs.* equilibrium pH. The slope of the plot is usually correlated to the number of protons exchanged during metal sorption (a concept derived from the analysis of pH effect in solvent extraction systems); in the case of rare earth sorption on chelating derivatives of chitosan (bearing EDTA and DTPA, ethylenediaminetetraacetic acid and diethylenetriaminepentaacetic acid, respectively) Inoue and Alam [66] reported a slope close to 3, which is consistent with the expected stoichiometry between protons exchanged on carboxylic groups of EDTA and DTPA and the trivalent charge of the REEs. In the present case, the conclusions are much more complex with a change in the slope close to pH 3.5. The corresponding stoichiometric ratios are close to 6.06:1 below pH 3.5 and to 1.64:1 above pH 3.5 (which corresponds to the order of magnitude of the pK_as of mannuronic acid and guluronic acid moieties). This complexity may be associated to different causes, such as (a) the presence of other functional groups (including sulfated polysaccharides present in the biomass, i.e., fucoidans, carrageenans, or amino-acids and other amine compounds) that have different acid-base properties, and different modes of reaction, but also (b) the possibility to exchange Ca(II) (instead of protons) with Pr(III). The equilibrium pH systematically increases during metal sorption (Fig. AM8, see Additional Material Section). However, the variation does not exceed 0.4 pH unit, probably due to proton binding on some of the reactive groups present on the biomass (more specifically amine groups). For limiting the risks of metal precipitation in the case of higher metal concentrations (such as the values used for achieving the saturation of the sorbent in the study of sorption isotherms) the pH is systematically adjusted at 4 for further experiments.

3.3. Uptake kinetics

The uptake kinetics have been investigated with AB beads for Pr (III) recovery (Fig. 3). The effect of drying method was carried out comparing the kinetic profiles for air-dried and freeze-dried materials (soaked overnight just before use). Under selected experimental conditions, a pseudo-equilibrium is reached within the first 8 h of contact. The residual sorption after 48 h of contact does not represent more than 8–9% of total sorption. There is a steep initial slope within the first hour of contact that represents a decrease in the relative concentration of about 40% (about 60% of the total sorption obtained at equilibrium). This first step corresponds to the sorption of the metal at the surface of AB beads (and within the first external layers of the sorbent) followed by a second phase that lasts for 6–7 h and corresponds to a slower sorption, which is associated to resistance to intraparticle diffusion.

Uptake kinetics are controlled by a series of mechanisms such as resistance to diffusion (both in the film surrounding the particles, and the intraparticle diffusion) in addition to the proper reaction rate (see Additional Material Section). In reactors with appropriate agitation the resistance to bulk diffusion can be neglected and the contribution of resistance to film diffusion is generally limited to the first minutes of contact. The kinetic profiles have been fitted by the pseudo-first order rate equation (PFORE, [58]), the pseudo-second order rate equation (PSORE, [59]) and the Crank equation (for intraparticle diffusion, [60]). Fig. 3 shows the modeling of experimental data with the PSORE, while the modeling with the Crank equation and the PFORE fit is presented in Fig. AM9 (see Additional Material Section). The PFORE and Crank equations fit well experimental profiles and better than the PFORE. Table 1 reports the parameters of the different models for Pr(III) sorption kinetics using two types of AB beads: air-dried beads (AD) and freeze-dried (FD) beads. This conclusion is confirmed by the comparison of estimated variances for PFORE and PSORE and by the much better approximation of the equilibrium sorption capacity ($q_{eq,exp}$) while using PSORE (errors being less than 3%) compared to PFORE (differences exceed 5%).

The characterization of materials (Section 3.1) showed that the freeze-drying allows maintaining the porous structure of the material better than the air-drying because of the restoration of particle size after soaking. This means that the drying method may influence the mass transfer properties of these materials. Actually this effect strongly depends on the type of metal and its chemical speciation in the solution (probably in relation with its ionic size). In

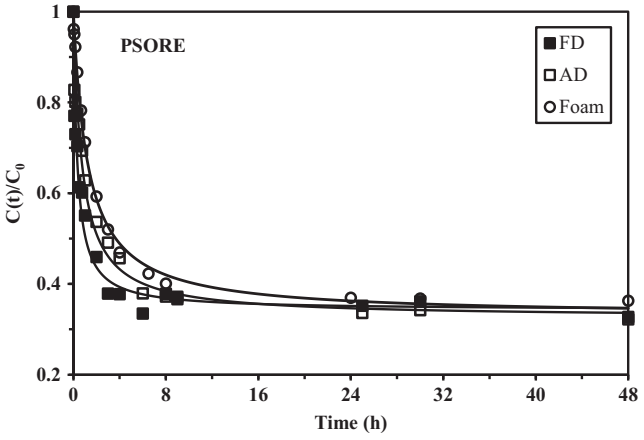

Fig. 3. Uptake kinetics for Pr(III) sorption using Algal Biomass beads – modeling with PSORE (freeze-dried: FD and air-dried: AD; pH 4.0; C_0: 50 mg Pr L^{-1}; SD: 0.3 g L^{-1}; v: 150 rpm; beads soaked overnight before use; flow rate: 5 mL min^{-1} for AB foams in recirculation mode; T: 20 °C).

Table 1
Uptake kinetics for Pr(III) sorption using Algal Biomass Beads – effect of drying mode (FD: freeze-drying, AD: air-drying) and kinetic modeling (Crank equation, PFORE and PSORE).

Model	Parameter	FD	AD	Foams
Experiment	$q_{eq,exp}$ (mg Pr g^{-1})/[mmol Pr g^{-1}]	116.5/0.83	119.7/0.85	100.8/0.72
PFORE	$q_{eq,calc}$ (mg Pr g^{-1})/[mmol Pr g^{-1}]	109.2/0.78	114.6/0.81	97.3/0.69
	$k_1 \times 10^2$ (min^{-1})	3.02	1.56	0.956
	EV	109.2	114.6	11.7
PSORE	$q_{eq,calc}$ (mg Pr g^{-1})/[mmol Pr g^{-1}]	113.9/0.81	119.0/0.84	106.1/0.75
	$k_2 \times 10^4$ (g mg^{-1} min^{-1})	4.37	1.86	1.26
	EV	48.2	48.8	4.69
Crank	$D_e \times 10^{10}$ (m^2 min^{-1})	4.04	0.62	n.d.
	EV	0.0224	0.0215	n.d.

EV: estimated variance; n.d.: not determined.

the case of Pb(II) and Cu(II) using similar materials the drying method did not significantly change the kinetic profiles [47]. The conclusion was completely different in the case of Pd(II) and Pt (IV) sorption [63]: the air-drying slowed-down mass transfer, especially for alginate beads (the effect was less marked for AB beads and AB/PEI beads). The formation of tetrachloropalladate and hexachloroplatinate anions may probably explain the more significant impact of drying method (and porous/structural properties) on the resistance to intraparticle diffusion and sorption kinetics. In the case of Pr(III) sorption the drying method has a very limited impact on sorption velocity: the kinetic profiles almost overlap; a slight time-shift of about 1 h is observed for AD materials compared to FD sorbent. The result suggests that although the air-dried sorbents are less porous than freeze-dried ones (possessing a smaller diameter, see in Section 3.1), the internal porosity built up by the re-hydration step is sufficient for readily diffusion of metal ions inside the sorbents (negligible diffusion hindrance). The ionic radius of Pb(II) (i.e., 1.19 Å; hydrated species under the form $Pb(H_2O)_6^{2+}$) is of the same order of magnitude than the value cited for Pr(III) (i.e., 1.179 Å, hydrated species under the form Pr $(H_2O)_9^{3+}$) [67]. The air-drying method halves the values of the apparent rate coefficients (k_1 and k_2) (Table 1). This is directly associated to slightly hindered diffusion properties: the diffusion coefficient (i.e., D_e) decreases from 4×10^{-10} m^2 min^{-1} for FD sorbent to 0.6×10^{-10} m^2 min^{-1} for air-dried material. This is several orders of magnitude lower than the molecular diffusivity of Pr(III) in water (i.e., 3.7×10^{-10} m^2 min^{-1}, [68]). This confirms the non-negligible effect of the resistance to intraparticle diffusion in the control of uptake kinetics. In the case of Pd(II) and Pt(IV) sorption using similar materials the air-drying also decreased the intraparticle diffusion coefficient from 1.4×10^{-10} m^2 min^{-1} to 0.24×10^{-10} m^2 min^{-1} for Pd(II) and from 1.82×10^{-10} m^2 min^{-1} to 0.58×10^{-10} m^2 min^{-1} for Pt(IV) [63]. Similar effect was observed for Cu(II) and Pb(II) sorption on AB beads: for Cu(II) the intraparticle diffusion coefficient decreases from 0.88×10^{-10} m^2 min^{-1} to 0.18×10^{-10} m^2 min^{-1}, and for Pb(II) from 1.35×10^{-10} m^2 min^{-1} to 0.24×10^{-10} m^2 min^{-1} [47]. In terms of diffusion coefficients in AB beads the metals can be ranked according: Pr(III) > Pt (IV) > Pd(II) ≈ Pb(II) > Cu(II). It is noteworthy that this ranking cannot be correlated to ionic size of hydrated species.

The uptake kinetics has also been determined in a recirculation mode with AB foams, under comparable experimental conditions. The kinetic profile is shown in Fig. 3 and Fig. AM9 (see Additional Material Section). It is noteworthy that the uptake kinetics is roughly superimposed to the curves obtained with AB beads: the AB foam curve is very close to the profile of air-dried AB beads, though the kinetics is slightly slower than for the beads. The comparison of apparent rate coefficients shows that the foams have slightly slower kinetic rates (consistently with Fig. 3): k_1 decreases from 1.56×10^{-2} min^{-1} for air-dried AB beads to 0.96×10^{-2} min^{-1} for AB foams while k_2 decreases from 1.86×10^4 g mg^{-1} min^{-1} to 1.26×10^4 g mg^{-1} min^{-1}, respectively. The sorption capacity at equilibrium is overestimated (106.1 mg Pr g^{-1} against 100.8 mg Pr g^{-1}) and slightly lower than the values reached with AB beads (i.e., 116.5 and 119.7 mg Pr g^{-1}). The conditioning of the biosorbents as a foam does not strongly impact kinetic behavior.

3.4. Sorption isotherms

The sorption isotherms represent the distribution of the solute between the liquid and solid phases for different solute concentrations. Several equations may be used for fitting these distribution curves including the Langmuir and the Freundlich equations [61]; these are the equations the most frequently used for describing sorption isotherms (see Additional Material Section for a reminder on these equations). The Freundlich equation is characterized by an exponential form (power-type function), which is not appropriate for fitting the asymptotic trend of sorption isotherms found in the case of Pr(III) removal by AB beads and AB foams (Fig. 4). However, the Langmuir equation fails to fit the experimental curves in the zone of higher curvature (dashed lines in Fig. 4) and the Sips equation was used. The Sips equation (also called Langmuir-Freundlich equation) introduces a supplementary parameter (i.e., n) that logically improves the quality of mathematical fit: this is confirmed by the good adjustment of the experimental profile with the Sips fit (solid lines) and the comparison of estimated variances in Table 2. The table reports the parameters of the Langmuir and Sips models for AB beads and AB foams and the experimental maximum sorption capacity. The value of q_m is sorption capacity at saturation of the monolayer for the Langmuir

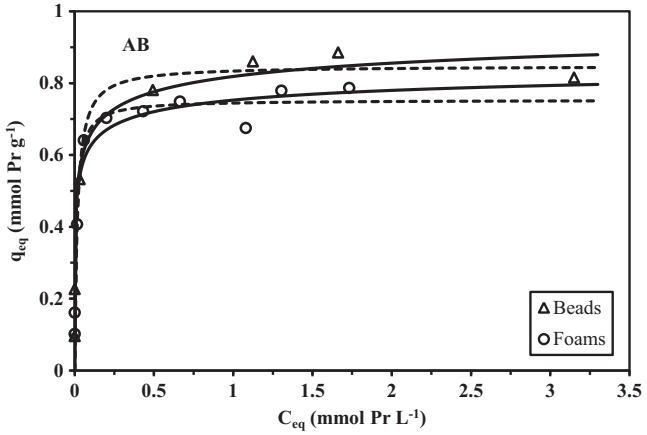

Fig. 4. Pr(III) sorption isotherms at pH 4 using Algal Biomass beads and foams – modeling with the Langmuir equation (dashed lines) and the Sips equation (solid lines) (; T: 20 °C).

Table 2
Sorption isotherms at pH 4 for Algal Biomass beads and foams – modeling with the Langmuir and the Sips equations.

Model	Parameters	AB beads	AB foams
Experimental	q_{max} (mmol Pr g^{-1})	0.89	0.79
	q_{max} (mg Pr g^{-1})	125.4	111.3
Langmuir	q_m (mmol Pr g^{-1})	0.85	0.75
	q_m (mg Pr g^{-1})	119.8	105.7
	b (L $mmol^{-1}$)	58.2	84.5
	EV	0.0117	0.0053
Sips	q_m (mmol Pr g^{-1})	1.03	0.89
	q_m (mg Pr g^{-1})	145.1	125.4
	b (L $mmol^{-1}$)	3.81	5.42
	n	2.96	2.75
	EV	0.0025	0.0025

equation is systematically slightly lower (by a few percent) than the experimental maximum sorption capacity (q_{max}; in the range 0.79–0.89 mmol Pr g^{-1}, or 111–125 mg Pr g^{-1}). It is noteworthy that the AB foams have slightly lower q_m and q_{max} values than AB beads. On the opposite hand, the corresponding q_m values in the Sips models slightly overestimate the q_{max}. The values of the coefficient b (related to the affinity of the sorbent for the target metal) for AB foams increase for both Langmuir and Sips models (in comparison with AB beads). For Langmuir equation the product $q_m \times b$ is analogous to a distribution coefficient (L g^{-1}) and represents the initial slope of the isotherm curve: this slope increases for AB foams (i.e., 63.4 L g^{-1}) compared with AB beads (i.e., 49.5 L g^{-1}).

However, in this study, although it is difficult to confirm the amount of the functional groups due to the complexity of the sorbents, the sorption isotherms (almost irreversible) give a steep rise when C_e is below 6 mg L^{-1} for beads and 8 mg L^{-1} for foams. In most cases (C_e > 8 mg L^{-1}), the binding mechanism is the unidentate bridging coordination; this is consistent with the results deduced from FTIR analysis.

Table AM2 (see Additional Material Section) reports Pr(III) sorption properties of a series of sorbents. Macroporous resin D72 (which bears sulfonic groups) has much higher sorption capacities than other sorbents. AB beads and foams show sorption levels comparable with those of conventional biosorbents: algal biomass [40,69], or fungal biomass [70] and much better than agriculture waste materials [71] or TVEX-PHOR resin [72].

3.5. Metal desorption and sorbent recycling using beads

Metal desorption from loaded sorbent may have two objectives: (a) the release of the metal for facilitating the re-use of the sorbent, and (b) the effect of concentration of the metal in a reduced volume for final valorization of the metal. In addition to the proper selectivity of the sorption mechanism, in the case of complex systems involving several metal ions, desorption may contribute to improve the selective separation of the metals. The sorbents collected during the investigation of the kinetics have been used for testing the desorption kinetics (Fig. AM10, see Additional Material Section). The acidic solution of $CaCl_2$ is used for removing Pr(III) from loaded AB beads: the acid is supposed to bring high concentration of protons that will displace the metal ions from the sorbent (at low pH the interaction between reactive groups such as carboxylate groups and Pr(III) ions is strongly depreciated) and this competition effect is completed by the action of Ca(II) ions that contribute to re-stabilize the sorbent (ionotropic gelation of carboxylate groups with Ca(II)). The comparison of desorption kinetics for air-dried and freeze-dried beads confirms (as already identified during the study of uptake kinetics) that the freeze-drying increases the kinetics of the desorption process: the complete removal of Pr(III) occurs within 0.5–1 h of contact for FD AB beads while for AD AB beads the contact time should be extended to 5–6 h.

Fig. AM11 (see Additional Material Section) shows the change in the sorption/desorption along five cycles of sorption/desorption using different volume ratios between the volumes used for sorption and desorption steps. This figure clearly shows that the decrease in both sorption and desorption efficiencies is relatively limited: at the fifth cycle the decrease in desorption efficiency remains below 6% for the two volumetric ratios while the sorption efficiency decreases by less than 4%. The main sorption/desorption mechanism that consists of Pr (III)/Ca(II) ion exchange has been confirmed by SEM-EDX results (see Section 3.1.). Adding calcium chloride (at the concentration of 0.05 M) to acid desorption agent not only helps to maintain the stability of the sorbents, but also contributes to the highly efficiency of desorption. In addition, FTIR analysis confirms that active functional groups are not significantly lost even after 5 cycles (see Section 3.1.). This explains that only a little reduction of the sorption capacity is observed. The calculated amount of Pr(III) remaining on the beads after 5 cycles is as low as 9 mg g^{-1} (after the last desorption step, data not shown). The two volumetric ratios show very similar results: the sorption efficiency is even better for the large $V_{sorpt.}/V_{des.}$ ratio; this may be explained by a weaker degradation of the sorbent due to the lower amount of strong acid solution. The materials are remarkably stable in terms of sorption/desorption properties when re-used for a minimum of 5 cycles.

Fig. AM12 (see Additional Material Section) addresses more specifically the determination of optimum conditions for combined high desorption efficiency (%) and high concentration factor (CF, ratio of metal concentration in the eluate over its concentration in the sorption step solution) when varying the volumetric ratio $V_{sorpt.}/V_{des.}$ on a larger scale (up to 40). As expected, the CF increases when the volume of eluate decreases. However, when the volumetric ratio exceeds 10 the efficiency of desorption progressively decreases. A good compromise between these parameters rises in the range: $V_{sorpt.}/V_{des.}$ 10–15 with desorption efficiency higher than 92% and a CF in the range 8–10.

3.6. Tests in dynamic systems using foams: sorption and desorption

The AB foams have been tested in dynamic systems. In this case the immobilized disc was not fed in a recirculation mode but in a single-pass mode at decreased flow rate in order to maintain the solution in contact with the foams for a sufficient time. The Fig. 5 shows the breakthrough curve for Pr(III) sorption on AB foam: the relative metal concentration at the outlet of the foam and the cumulative amount of Pr(III) bound to the foam are plotted against contact time. The sorption efficiency is calculated (close to 57%) at quasi-saturation of the sorbent (taking into account the amount of metal fed into the column and the amount effectively bound on the support). The sorption capacity calculated by the mass balance gives a sorption capacity close to 78 mg Pr g^{-1} (0.56 mmol Pr g^{-1}) that can be compared to the sorption capacity calculated from sorption isotherms for a residual concentration corresponding to the feed concentration (i.e., 0.62 mmol Pr g^{-1} or 87.6 mg Pr g^{-1}). The slight decrease can be explained by the incomplete saturation of the sorbent ($C(t)/C_0$: 0.88). Several models exist for the modeling of breakthrough such as the Thomas equation [73] and the Adams-Bohart model [74]. Yan et al. [62] suggest using an alternative model based on logistic function for getting a better approximation of the breakthrough curves at the beginning and ending steps of the breakthrough curves. The so-called Yan equation is reported in Additional Material Section [75], in Fig. 5 the dotted line represents the modeling of the breakthrough curve with the following equation:

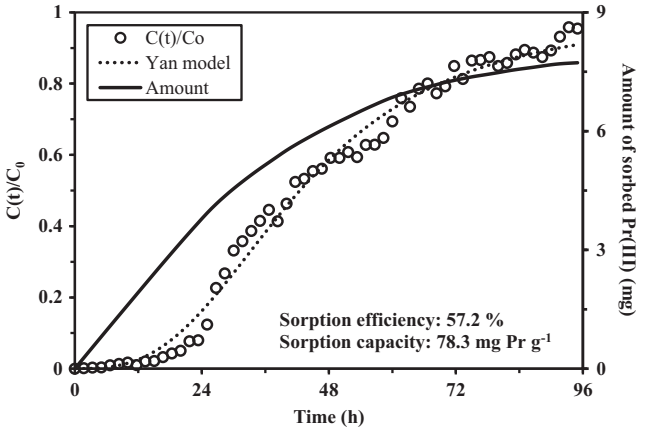

Fig. 5. Breakthrough curve for Pr(III) sorption through Algal Biomass foam – evolutions of $C(t)/C_0$ and amount of Pr(III) sorbed *vs.* time (Sorbent amount: 101.9 mg; C_0: 15 mg Pr L^{-1}; pH 4; flow rate: 0.2 mL min^{-1}; T: 20 °C; dotted line: BC fit with Yan model).

$$\frac{C(t)}{C_0} = 1 - \frac{1}{1 + (\beta' \times t)^{\alpha}} \quad (1)$$

with $\alpha = 2.86991$ and $\beta' = 3.919 \times 10^{-4}$.

This corresponds to $q_{yan} = 69.8$ mg Pr g^{-1}. This value is lower than the value obtained by the mass balance on the experimental data from breakthrough curves (i.e., 78.3 mg Pr g^{-1}) and even lower than the expected value deduced from sips equation (i.e., 87.7 mg Pr g^{-1}). It is noteworthy that the sorbent was not fully saturated since the relative outlet concentration after passing a volume of 1.1 L of Pr(III) solution did not exceed 95%: this may explain the underestimated value of sorption capacity at pseudo-saturation in the column.

The efficiency of desorption reaches 93% with a concentration factor (CF) that is close to 8 (Fig. 6). The CF was calculated as the ratio of the equivalent eluate concentration (i.e., 112 mg Pr L^{-1}) after passing 62.5 mL of eluent in the column to the inlet concentration (i.e., 13.5 mg Pr L^{-1}). Indeed, 62.5 mL of eluent are sufficient for achieving about 98% of total desorption: the eluate concentration being below 2 mg Pr L^{-1} for the subsequent eluate fractions. The peak concentration obtained within the first fraction of 12.5 mL reached up to 425 mg Pr L^{-1}.

The continuous mode reveals quite efficient for the recovery, desorption and concentration of Pr(III) using low flow rate (i.e., 0.2 mL min^{-1}, 12 mL h^{-1} and superficial flow velocity close to 2.44×10^{-2} m h^{-1}) to achieve a sufficient contact time in the foam.

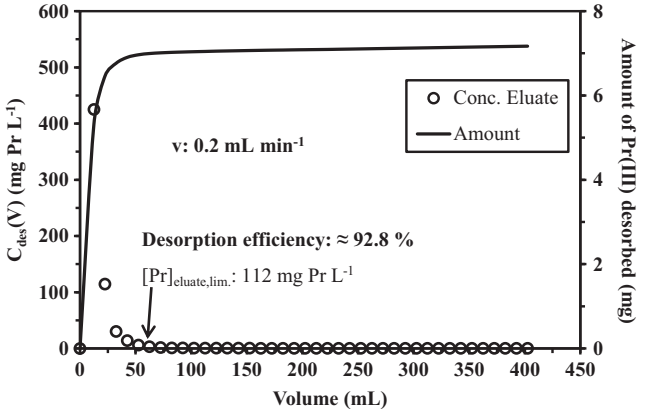

Fig. 6. Pr(III) desorption from metal-loaded Algal Biomass foam in continuous mode – evolutions of eluate concentration (C_{des}) and amount of Pr(III) desorbed *vs.* volume of eluent solution (Pr-loaded sorbent collected from Fig. AM5 experiment; desorption using 2 M HCl/0.05 M $CaCl_2$ solutions; flow rate: 0.2 mL min^{-1}; T: 20 °C).

4. Conclusion

SEM-EDX analysis shows the macro-porous structure of the materials and the homogeneous distribution of Pr(III) in the material: all reactive groups remain available and accessible. FTIR analysis confirms the contribution of carboxylic groups in the binding of Pr(III); the detection of S element on the SEM-EDX spectra shows that sulfonic groups are also present and may contribute to metal binding. The mechanisms involved in praseodymium uptake consist of the ion-exchange of Pr(III) with Ca(II) ions (ionotropic gelation agent for the synthesis of AB "hydrogels"). The co-existence of different reactive groups and the possibility for metal to exchange also with protons on biosorbents may explain the difficulty in correlating distribution coefficient with pH variation (non-consistent with the stoichiometric ratio of ion charges).

The one-pot extraction and shaping of algal biomass (AB, without addition of encapsulating agent) and the conditioning of the material as beads and foams offer promising processes for the elaboration of biosorbents with improved processing properties such as fixed-bed column systems (contrary to ribbon-like or granular shape of original materials). The sorption properties of the materials for Pr(III) reveal comparable to those of other algal biosorbents. The sorption isotherms are well described by the Langmuir and the Sips equations and the maximum sorption capacities are around 110–120 mg Pr(III) g^{-1}. The uptake kinetics for AB beads are fitted by the pseudo-second order rate equation (PSORE) and by the Crank equation; they are hardly affected by the mode of drying (freeze-dried against air-dried). In the case of AB foams the PSORE fits well experimental profile. Metal desorption is successfully operated both in batch tests (for AB beads) and fixed-bed columns (for AB foams) using 2 M HCl/0.05 M $CaCl_2$. Desorption is fast, efficient (higher than 95%) and the recycling of the sorbent is possible for at least 5 cycles of sorption/desorption. A concentration factor of 8–10 can easily be achieved while selecting appropriate volumes of eluent.

Acknowledgements

S. Wang acknowledges the China Scholarship Council (CSC, China, Grant N° 20156660002) for providing PhD fellowship. M. Hamza acknowledges the financial support from French Government (French Embassy in Egypt, Institut Français d'Egypte, IFE) for his research training period at Ecole des mines d'Alès. T. Vincent and E. Guibal acknowledge European Union's Seventh Framework Programme (FP7/2007-2013) since these results are indirectly derived from a research project (BIOMETAL-DEMO) funded by the FP7 Programme managed by REA-Research Executive Agency (http://ec.europa.eu/research/rea) under Grant N° 699101.

References

[1] N. Haque, A. Hughes, S. Lim, C. Vernon, Rare earth elements: overview of mining, mineralogy, uses, sustainability and environmental impact, Resources 3 (2014) 614.

[2] G. Charalampides, K.I. Vatalis, B. Apostoplos, B. Ploutarch-Nikolas, Rare earth elements: Industrial applications and economic dependency of Europe, Procedia Econ. Finance 24 (2015) 126–135.

[3] M.I. Aly, B.A. Masry, M.S. Gasser, N.A. Khalifa, J.A. Daoud, Extraction of Ce (IV), Yb (III) and Y(III) and recovery of some rare earth elements from Egyptian

monazite using CYANEX 923 in kerosene, Int. J. Miner. Process. 153 (2016) 71–79.
[4] K. Binnemans, P.T. Jones, B. Blanpain, T. Van Gerven, Y. Yang, A. Walton, M. Buchert, Recycling of rare earths: a critical review, J. Clean. Prod. 51 (2013) 1–22.
[5] C. Tunsu, M. Petranikova, M. Gergoric, C. Ekberg, T. Retegan, Reclaiming rare earth elements from end-of-life products: a review of the perspectives for urban mining using hydrometallurgical unit operations, Hydrometallurgy 156 (2015) 239–258.
[6] L.S. Morf, R. Gloor, O. Haag, M. Haupt, S. Skutan, F. Di Lorenzo, D. Boeni, Precious metals and rare earth elements in municipal solid waste – sources and fate in a Swiss incineration plant, Waste Manage. (Oxf.) 33 (2013) 634–644.
[7] M. Bigum, L. Brogaard, T.H. Christensen, Metal recovery from high-grade WEEE: a life cycle assessment, J. Hazard. Mater. 207 (2012) 8–14.
[8] S.R. Mueller, P.A. Waeger, R. Widmer, I.D. Williams, A geological reconnaissance of electrical and electronic waste as a source for rare earth metals, Waste Manage. (Oxf.) 45 (2015) 226–234.
[9] P. Meshram, B.D. Pandey, T.R. Mankhand, Process optimization and kinetics for leaching of rare earth metals from the spent Ni-metal hydride batteries, Waste Manage. (Oxf.) 51 (2016) 196–203.
[10] M.K. Jha, A. Kumari, R. Panda, J. Rajesh Kumar, K. Yoo, J.Y. Lee, Review on hydrometallurgical recovery of rare earth metals, Hydrometallurgy 165 (Part 1) (2016) 2–26.
[11] F. Xie, T.A. Zhang, D. Dreisinger, F. Doyle, A critical review on solvent extraction of rare earths from aqueous solutions, Miner. Eng. 56 (2014) 10–28.
[12] D. Kim, L.E. Powell, L.H. Delmau, E.S. Peterson, J. Herchenroeder, R.R. Bhave, Selective extraction of rare earth elements from permanent magnet scraps with membrane solvent extraction, Environ. Sci. Technol. 49 (2015) 9452–9459.
[13] I. Anastopoulos, A. Bhatnagar, E.C. Lima, Adsorption of rare earth metals: a review of recent literature, J. Mol. Liq. 221 (2016) 954–962.
[14] M.M. Yusoff, N.R.N. Mostapa, M.S. Sarkar, T.K. Biswas, M.L. Rahman, S.E. Arshad, M.S. Sarjadi, A.D. Kulkarni, Synthesis of ion imprinted polymers for selective recognition and separation of rare earth metals, J. Rare Earths 35 (2017) 177–186.
[15] T. Ogata, H. Narita, M. Tanaka, Adsorption behavior of rare earth elements on silica gel modified with diglycol amic acid, Hydrometallurgy 152 (2015) 178–182.
[16] N. Das, D. Das, Recovery of rare earth metals through biosorption: an overview, J. Rare Earths 31 (2013) 933–943.
[17] Z. Ren, X. Xu, X. Wang, B. Gao, Q. Yue, W. Song, L. Zhang, H. Wang, FTIR, Raman, and XPS analysis during phosphate, nitrate and Cr (VI) removal by amine cross-linking biosorbent, J. Colloid Interface Sci. 468 (2016) 313–323.
[18] E. Platero, M.E. Fernandez, P.R. Bonelli, A.L. Cukierman, Graphene oxide/alginate beads as adsorbents: Influence of the load and the drying method on their physicochemical-mechanical properties and adsorptive performance, J. Colloid Interface Sci. 491 (2017) 1–12.
[19] R. Lagoa, J.R. Rodrigues, Evaluation of dry protonated calcium alginate beads for biosorption applications and studies of lead uptake, Appl. Biochem. Biotechnol. 143 (2007) 115–128.
[20] S.K. Papageorgiou, F.K. Katsaros, E.P. Kouvelos, J.W. Nolan, H. Le Deit, N.K. Kanellopoulos, Heavy metal sorption by calcium alginate beads from *Laminaria digitata*, J. Hazard. Mater. 137 (2006) 1765–1772.
[21] W. Plazinski, Sorption of lead, copper, and cadmium by calcium alginate. Metal binding stoichiometry and the pH effect, Environ. Sci. Pollut. Res. 19 (2012) 3516–3524.
[22] B. An, H. Son, J. Chung, J.W. Choi, S.H. Lee, S.W. Hong, Calcium and hydrogen effects during sorption of copper onto an alginate-based ion exchanger: batch and fixed-bed column studies, Chem. Eng. J. 232 (2013) 51–58.
[23] S. Kwiatkowska-Marks, M. Wojcik, Removal of cadmium (II) from aqueous solutions by calcium alginate beads, Sep. Sci. Technol. 49 (2014) 2204–2211.
[24] H.J. Hong, J. Ryu, I.S. Park, T. Ryu, K.S. Chung, B.G. Kim, Investigation of the strontium (Sr(II)) adsorption of an alginate microsphere as a low-cost adsorbent for removal and recovery from seawater, J. Environ. Manage. 165 (2016) 263–270.
[25] Y. Kuang, J. Du, R. Zhou, Z. Chen, M. Megharaj, R. Naidu, Calcium alginate encapsulated Ni/Fe nanoparticles beads for simultaneous removal of Cu (II) and monochlorobenzene, J. Colloid Interface Sci. 447 (2015) 85–91.
[26] Z. Tang, S. Peng, S. Hu, S. Hong, Enhanced removal of bisphenol-AF by activated carbon-alginate beads with cetyltrimethyl ammonium bromide, J. Colloid Interface Sci. 495 (2017) 191–199.
[27] S. Cataldo, A. Gianguzza, M. Merli, N. Muratore, D. Piazzese, M.L.T. Liveri, Experimental and robust modeling approach for lead (II) uptake by alginate gel beads: Influence of the ionic strength and medium composition, J. Colloid Interface Sci. 434 (2014) 77–88.
[28] D. Song, S.-J. Park, H.W. Kang, S.B. Park, J.-I. Han, Recovery of lithium(I), strontium(II), and lanthanum(III) using Ca-alginate beads, J. Chem. Eng. Data 58 (2013) 2455–2464.
[29] F. Wang, J. Zhao, W. Li, H. Zhou, X. Yang, N. Sui, H. Liu, Preparation of several alginate matrix gel beads and their adsorption properties towards rare earths III, Waste Biomass Valorization 4 (2013) 665–674.
[30] F. Wang, J. Zhao, X. Wei, F. Huo, W. Li, Q. Hu, H. Liu, Adsorption of rare earths (III) by calcium alginate-poly glutamic acid hybrid gels, J. Chem. Technol. Biotechnol. 89 (2014) 969–977.
[31] F.C. Wang, J.M. Zhao, F. Pan, H.C. Zhou, X.F. Yang, W.S. Li, H.Z. Liu, Adsorption properties toward trivalent rare earths by alginate beads doping with silica, Ind. Eng. Chem. Res. 52 (2013) 3453–3461.
[32] D. Wu, L. Zhang, L. Wang, B. Zhu, L. Fan, Adsorption of lanthanum by magnetic alginate-chitosan gel beads, J. Chem. Technol. Biotechnol. 86 (2011) 345–352.
[33] S. Xu, Z. Wang, Y. Gao, S. Zhang, K. Wu, Adsorption of rare earths(III) using an efficient sodium alginate hydrogel cross-linked with poly-gamma-glutamate, Plos One 10 (2015).
[34] E. Romera, F. Gonzalez, A. Ballester, M.L. Blazquez, J.A. Munoz, Comparative study of biosorption of heavy metals using different types of algae, Bioresour. Technol. 98 (2007) 3344–3353.
[35] P.X. Sheng, Y.-P. Ting, J.P. Chen, L. Hong, Sorption of lead, copper, cadmium, zinc, and nickel by marine algal biomass: characterization of biosorptive capacity and investigation of mechanisms, J. Colloid Interface Sci. 275 (2004) 131–141.
[36] C. Boschi, H. Maldonado, M. Ly, E. Guibal, Cd (II) biosorption using *Lessonia kelps*, J. Colloid Interface Sci. 357 (2011) 487–496.
[37] M.C. Palmieri, O. Garcia Jr, P. Melnikov, Neodymium biosorption from acidic solutions in batch system, Process Biochem. 36 (2000) 441–444.
[38] M.C. Palmieri, B. Volesky, O. Garcia, Biosorption of lanthanum using *Sargassum fluitans* in batch system, Hydrometallurgy 67 (2002) 31–36.
[39] N. Ishii, K. Tagami, S. Uchida, Removal of rare earth elements by algal flagellate *Euglena gracilis*, J. Alloys Compd. 408 (2006) 417–420.
[40] R.C. Oliveira, C. Jouannin, E. Guibal, O. Garcia Jr., Samarium(III) and praseodymium(III) biosorption on *Sargassum sp.*: batch study, Process Biochem. 46 (2011) 736–744.
[41] A.M. Zoll, J. Schijf, A surface complexation model of YREE sorption on *Ulva lactuca* in 0.05–5.0 M NaCl solutions, Geochim. Cosmochim. Acta 97 (2012) 183–199.
[42] F.A. Abu Al-Rub, M.H. El-Naas, F. Benyahia, I. Ashour, Biosorption of nickel on blank alginate beads, free and immobilized algal cells, Process Biochem. 39 (2004) 1767–1773.
[43] P.T. Wang, Z.Y. Li, J. Bai, Y.H. Lang, H. Hu, Optimization of microalgal bead preparation with *Scenedesmus obliquus* for both nutrient removal and lipid production, Ecol. Eng. 92 (2016) 236–242.
[44] A. Ruiz-Marin, L.G. Mendoza-Espinosa, T. Stephenson, Growth and nutrient removal in free and immobilized green algae in batch and semi-continuous cultures treating real wastewater, Bioresour. Technol. 101 (2010) 58–64.
[45] Y.X. Shang, X.F. Yu, Screening of algae material as a filter for heavy metals in drinking water, Algal Res. 12 (2015) 258–261.
[46] I.A. Erkaya, M.Y. Arica, A. Akbulut, G. Bayramoglu, Biosorption of uranium(VI) by free and entrapped *Chlamydomonas reinhardtii*: kinetic, equilibrium and thermodynamic studies, J. Radioanal. Nucl. Chem. 299 (2014) 1993–2003.
[47] S. Wang, T. Vincent, C. Faur, E. Guibal, Alginate and algal-based beads for the sorption of metal cations: Cu(II) and Pb(II), Int. J. Mol. Sci. 17 (2016).
[48] S. Wang, T. Vincent, C. Faur, E. Guibal, Modeling competitive sorption of lead and copper ions onto alginate and greenly prepared algal-based beads, Bioresour. Technol. 231 (2017) 26–35.
[49] S. Wang, T. Vincent, J.-C. Roux, C. Faur, E. Guibal, Pd (II) and Pt (IV) sorption using alginate and algal-based beads, Chem. Eng. J. 313 (2017) 567–579.
[50] S.V. Madihally, H.W.T. Matthew, Porous chitosan scaffolds for tissue engineering, Biomaterials 20 (1999) 1133–1142.
[51] C. Vincent, Y. Barre, T. Vincent, J.M. Taulemesse, M. Robitzer, E. Guibal, Chitin-Prussian blue sponges for Cs(I) recovery: From synthesis to application in the treatment of accidental dumping of metal-bearing solutions, J. Hazard. Mater. 287 (2015) 171–179.
[52] E. Guibal, S. Cambe, S. Bayle, J.-M. Taulemesse, T. Vincent, Silver/chitosan/cellulose fibers foam composites: From synthesis to antibacterial properties, J. Colloid Interface Sci. 393 (2013) 411–420.
[53] C. Vincent, A. Hertz, T. Vincent, Y. Barre, E. Guibal, Immobilization of inorganic ion-exchanger into biopolymer foams – application to cesium sorption, Chem. Eng. J. 236 (2014) 202–211.
[54] D.J. McHugh, Production and utilization of products from commercial seaweeds. Chapter 2 – production, properties and uses of alginates., in: FAO (Ed.) FAO Fisheries Technical Papers, FAO, Rome (Italy), 1987, pp. 58–115.
[55] C. Bertagnolli, A.P.D.M. Espindola, S.J. Kleinuebing, L. Tasic, M.G. Carlos da Silva, *Sargassum filipendula* alginate from Brazil: seasonal influence and characteristics, Carbohydr. Polym. 111 (2014) 619–623.
[56] P. Agulhon, M. Robitzer, L. David, F. Quignard, Structural regime identification in ionotropic alginate gels: influence of the cation nature and alginate structure, Biomacromolecules 13 (2012) 215–220.
[57] M.V. Lopez-Ramon, F. Stoeckli, C. Moreno-Castilla, F. Carrasco-Marin, On the characterization of acidic and basic surface sites on carbons by various techniques, Carbon 37 (1999) 1215–1221.
[58] S. Lagergren, About the theory of so-called adsorption of soluble substances, Kungliga Svenska Vetenskapsakademiens 24 (1898) 1–39.
[59] Y.S. Ho, G. McKay, Pseudo-second order model for sorption processes, Process Biochem. 34 (1999) 451–465.
[60] J. Crank, The Mathematics of Diffusion, second. ed., Oxford University Press, Oxford, U.K., 1975.
[61] C. Tien, Adsorption Calculations and Modeling, Butterworth-Heinemann, Newton, MA, 1994.
[62] G.Y. Yan, T. Viraraghavan, M. Chen, A new model for heavy metal removal in a biosorption column, Adsorpt. Sci. Technol. 19 (2001) 25–43.

[63] S. Wang, T. Vincent, J.-C. Roux, C. Faur, E. Guibal, Pd(II) and Pt(IV) sorption using alginate and algal-based beads, Chem Eng. J. (2017), http://dx.doi.org/10.1016/j.cej.2016.12.039.
[64] S.K. Papageorgiou, E.P. Kouvelos, E.P. Favvas, A.A. Sapalidis, G.E. Romanos, F.K. Katsaros, Metal-carboxylate interactions in metal-alginate complexes studied with FTIR spectroscopy, Carbohydr. Res. 345 (2010) 469–473.
[65] A. Haug, Dissociation of alginic acid, Acta Chem. Scand. 15 (1961) 950–952.
[66] K. Inoue, S. Alam, Refining and mutual separation of rare earths using biomass wastes, JOM 65 (2013) 1341–1347.
[67] I. Persson, Hydrated metal ions in aqueous solution: how regular are their structures?, Pure Appl Chem. 82 (2010) 1901–1917.
[68] Y. Marcus, Ion Properties, Marcel Dekker Inc, New York, NY, 1997.
[69] K. Vijayaraghavan, J. Jegan, Entrapment of brown seaweeds (*Turbinaria conoides* and *Sargassum wightii*) in polysulfone matrices for the removal of praseodymium ions from aqueous solutions, J. Rare Earths 33 (2015) 1196–1203.
[70] L. Philip, L. Iyengar, C. Venkobachar, Biosorption of U, La, Pr, Nd, Eu and Dy by *Pseudomonas aeruginosa*, J. Ind. Microbiol. Biotechnol. 25 (2000) 1–7.
[71] J.S.C. Varshini, D. Das, N. Das, Optimization of parameters for praseodymium (III) biosorption onto biowaste materials using response surface methodology: equilibrium, kinetic and regeneration studies, Ecol. Eng. 81 (2015) 321–327.
[72] S.I. El-Dessouky, E.A. El-Sofany, J.A. Daoud, Studies on the sorption of praseodymium (III), holmium (III) and cobalt (II) from nitrate medium using TVEX-PHOR resin, J. Hazard. Mater. 143 (2007) 17–23.
[73] C. Xiong, J. Zhu, C. Shen, Q. Chen, Adsorption and desorption of praseodymium (III) from aqueous solution using D72 resin, Chin. J. Chem. Eng. 20 (2012) 823–830.
[74] Y. Long, D. Lei, J. Ni, Z. Ren, C. Chen, H. Xu, Packed bed column studies on lead (II) removal from industrial wastewater by modified *Agaricus bisporus*, Bioresour. Technol. 152 (2014) 457–463.
[75] M. Ghasemi, A.R. Keshtkar, R. Dabbagh, S.J. Safdari, Biosorption of uranium(VI) from aqueous solutions by Ca-pretreated *Cystoseira indica* alga: breakthrough curves studies and modeling, J. Hazard. Mater. 189 (2011) 141–149.